Cellulose (2012) 19:401–410
DOI 10.1007/s10570-011-9629-5

Ultra porous nanocellulose aerogels as separation medium for mixtures of oil/water liquids

Nicholas Tchang Cervin · Christian Aulin · Per Tomas Larsson · Lars Wågberg

Received: 15 August 2011 / Accepted: 23 November 2011 / Published online: 17 December 2011

Abstract A novel type of sponge-like material for the separation of mixed oil and water liquids has been prepared by the vapour deposition of hydrophobic silanes on ultra-porous nanocellulose aerogels. To achieve this, a highly porous (>99%) nanocellulose aerogel with high structural flexibility and robustness is first formed by freeze-drying an aqueous dispersion of the nanocellulose. The density, pore size distribution and wetting properties of the aerogel can be tuned by selecting the concentration of the nanocellulose dispersion before freeze-drying. The hydrophobic light- weight aerogels are almost instantly filled with the oil phase when selectively absorbing oil from water, with a capacity to absorb up to 45 times their own weight in oil. The oil can also be drained from the aerogel and the aerogel can then be reused for a second absorption cycle.

Keywords Absorption · Aerogel · Cellulose · Desorption · Oleophilic · Separation · Superhydrophobic

Introduction

Aerogels are ultra-light, highly porous materials typically manufactured by subjecting a wet-gel precursor to critical-point-drying (CPD) or lyophilization (freeze-drying) in order to remove liquid without collapsing the network. Microscopically, aerogels are composed of tenuous networks of clustered nanoparticles, and the materials often have unique properties, including very high strength-to-density and surface-area-to-volume ratios. To date most aerogels are fabricated from silica (Hrubesh 1998) or pyrolized organic polymers (Pekala 1989; Pekala et al. 1998). A typical problem has been their fragility which has limited their use in applications where robustness is needed. To overcome this problem, aerogels based on native cellulose nanofibril networks were recently introduced, which are less brittle and more flexible in facile and relevant ways (Paakko et al. 2008). The long and entangled native cellulose nanofibrils form an aerogel network with a fibrillar morphology and strong molecular interactions including both van der Waals

Electronic supplementary material The online version of this article (doi:10.1007/s10570-011-9629-5) contains supplementary material, which is available to authorized users.

N. T. Cervin (✉) · C. Aulin · P. T. Larsson · L. Wågberg
Wallenberg Wood Science Center, KTH Royal Institute of Technology, Teknikringen 56, 10044 Stockholm, Sweden
e-mail: tchang@kth.se

C. Aulin · P. T. Larsson · L. Wågberg
Innventia AB, Box 5604, 11486 Stockholm, Sweden

P. T. Larsson · L. Wågberg
Department of Fibre and Polymer Technology, School of Chemical Science and Engineering, KTH Royal Institute of Technology, Teknikringen 56, 10044 Stockholm, Sweden

interactions and hydrogen bonds, and they are therefore suitable for various templating applications (Aulin et al. 2010b; Kettunen et al. 2011; Paakko et al. 2008).

The nanocellulose fibrils, used for preparation of these aerogels, i.e. cellulosic I fibrils disintegrated from the wood-fibre cell walls, are derived from renewable sources and are very interesting as nano-sized building blocks due to their high aspect ratio (Paakko et al. 2007), high specific surface area and very attractive mechanical properties (Henriksson et al. 2008). The preparation of nanocellulose from wood was originally described by Turbak et al. (1983) and by Herrick et al. (1983) more than two decades ago. Through a homogenization process, wood pulp is disintegrated to give a material in which the fibers are degraded and opened into their sub-structural units. The energy consumption for the preparation of this NanoFibrillated Cellulose (NFC) was however large and this prevented further application of this otherwise interesting material. Recently it was however shown that a pretreatment of the fibres with a combination of enzymatic and mechanical treatment before high-pressure homogenization (Paakko et al. 2007) led to an energy-efficient production of NFC. It was also shown that a pre-charging of the fibre wall before the high-pressure homogenization, either by carboxymethylation (Wagberg et al. 2008) or with *N*-(2,3 epoxypropyl)trimethylammonium chloride (Aulin et al. 2010a) facilitate the homogenization process due to the swelling of the fibre wall by these anionic or cationic charges. Due to the higher electrostatic repulsion between the liberated fibrils, this also facilitated the preparation of smaller and more uniformly sized NFC with lateral dimensions of about 5 nm and a length of more than 1.5 μm (Wagberg et al. 2008). The efficient preparation of this new type of nanofiber has created a large interest in the preparation of new nanostructured materials for novel applications (Nakagaito and Yano 2004; Saito et al. 2006; Siqueira et al. 2009; Yano et al. 2005).

If the nanocellulose dispersions are freeze-dried, aerogels with very high porosity, typically above 98 vol% are produced and the network morphology and density of these aerogels can be tuned by the selected freeze-drying conditions (Paakko et al. 2008; Sehaqui et al. 2010) and the concentration of the nanocellulose dispersions (Aulin et al. 2010b).

Since these types of aerogel have a large specific surface area (Aulin et al. 2010b; Sehaqui et al. 2010) and remarkable mechanical properties (Sehaqui et al. 2010) they are highly interesting as starting materials for various types of functional materials. In the present work, the nanocellulose aerogels have been modified with silanes using vapour deposition, by which the surfaces of the aerogels become highly hydrophobic, with contact angles >150°. These aerogels selectively absorb oils and thus function as light-weight porous media for the separation of oil and water mixtures. The absorption capacity can be tuned by adjusting the porosity and the nano/micro porous network structure of the material. The low weight, high porosity and tunable absorption properties of the nanocellulose aerogels make them promising candidates for environmental applications such as sorption, filtration and separation.

This work was first published at the 241st National Meeting and Exposition of the American-Chemical-Society (ACS) in Anaheim 2011 (Cervin et al. 2011). During the finishing preparation of the manuscript a similar work was published by Ikkala et al. on oil-absorbing cellulose aerogels using TiO_2 nanoparticles as surface modification. The main difference between these two research projects is that they treat the whole aerogel with particles whereas in our case only the outermost part is being treated. They do not show any details on absorption and pore structure and there is no quantification of oil-absorbing capacity given. The spent work is more extensive and adds to the information given by Korhonen et al. (2011).

Experimental

Materials

A commercial sulfite softwood-dissolving pulp (Domsjö Dissolving Pulp; Domsjö Fabriker AB, Domsjö, Sweden) made from 60% Norwegian spruce (Picea abies) and 40% Scotch pine (Pinus sylvestris), with a hemicellulose content of 4.5% and a lignin content of 0.6% was used for manufacturing NFC consisting of mainly cellulose I nanofibers with cross-sectional dimensions of 5–20 nm and lengths in the micrometer regime. (Aulin et al. 2010b) Octyltrichlorosilane used was purchased from Sigma Aldrich (Octyltrichlorosilane 97%) and the Hexadecane (Hexadecane 99%) was purchased from Alfa Aesar. The Octyltrichlorosilane and the Hexadecane were both used as shipped from the supplier.

Methods

Preparation of NFC

The NFC was prepared at Innventia AB, Stockholm, Sweden, with the aid of a high-pressure homogenization technique using a carboxymethylation pretreatment of the fibers. The never-dried fibers were first dispersed in deionized water at 10,000 revolutions in an ordinary laboratory reslusher. The fibers were than solvent-changed to ethanol by washing the fibers in ethanol four times with intermediate filtration. The fibers were then impregnated for 30 min with a solution of 10 g of monochloroacetic acid in 500 mL of isopropanol. These fibers were added in portions to a solution of NaOH, methanol and isopropanol that had been heated to just below its boiling point, and the carboxymethylation reaction was allowed to continue for 1 h. Following the carboxymethylation step, the fibers were filtered and washed in three steps: first with deionized water, then with acetic acid (0.1 M) and finally with deionized water again. The fibers were then impregnated with a $NaHCO_3$ solution (4 wt% solution) in order to convert the carboxyl groups to their sodium form. Finally, the fibers were washed with deionized water and drained on a Büchner funnel. After this treatment, the fibers were passed through a high-pressure homogenizer (Microfluidizer M-110EH, Microfluidics Corp). The homogenizer was equipped with two chambers of different sizes connected in series (200 and 100 μm). Full homogenization was achieved with a single pass at a fiber consistency of 2 wt%.

Preparation of NFC aerogels

NFC dispersions with different contents of nanofibers were prepared by diluting a 2 wt% NFC dispersion with deionized water followed by mixing (8,000 rpm) in an Ultra Turrax mixer (IKA D125 Basic, Germany) for 5 min. Four different consistencies were used, 0.5, 1, 1.5 and 2 wt% NFC in aqueous solution. The aqueous dispersion was frozen in an aluminum mold by submersion in liquid nitrogen. The frozen mould was then transferred to a vacuum oven at −90 °C (Christ ALPHA 2–4 LD plus) and the sample was kept frozen during drying at a pressure of approximately 0,040 mbar. The drying was typically finished within 48 h.

Silanization

In order to make the hydrophilic NFC aerogels hydrophobic, they were treated with octyltrichlorosilane through vapor phase deposition. The samples were placed on a copper grid located above the liquid silane, the liquid silane was then heated to 30 °C below its boiling point i.e., 180 °C, and the aerogels were treated for 30 min.

Automated pore volume distribution measurement

A TRI/Autoporosimeter version 2008–12 (TRI/Princeton, Princeton, USA) (Miller and Tyomkin 1994) was used to measure the cumulative pore volume distribution using hexadecane as liquid. The membrane cut-off radius was 1.2 μm, which effectively limited the smallest measurable pore radius to about 5 μm. Cumulative pore volume distributions were recorded using 19 pressure points corresponding to pore radii in the range of 500–5 μm. The pore radii corresponding to a certain chamber gas pressure was calculated using the relation:

$$\Delta P = \frac{2\gamma \cos\theta}{r}$$

where γ is the liquid–gas surface tension of the liquid used, in this case hexadecane (27 mN/m), θ is the liquid–solid contact angle ($\cos\theta = 1$, full wetting is assumed), ΔP is the difference between the chamber gas pressure and atmospheric pressure and r is the pore radius.

Three complete Automated pore volume distribution measurement (APVD) desorption/sorption cycles were recorded for each material. The liquid mass contained in pores smaller than 5 μm was determined gravimetrically. The APVD is equipped with a valve separating the membrane/sample system from the liquid reservoir situated on the analytical balance. Closing this valve before depressurising the sample chamber makes it possible to determine gravimetrically the amount of liquid present in a sample at any chosen gas pressure. The amount of liquid trapped in the pores below 5 μm can also be seen in Figs. 4 and 6 where the end point of the desorption curve of cycle 1 corresponds to the gravimetrically value.

Contact angle measurement

A Contact angle measurement (CAM) 200 (KSV Instruments Ltd, Helsinki, Finland) contact angle goniometer was used for advancing contact angle measurements. The software delivered by the instrument manufacturer calculates the contact angle on the basis of a numerical solution from measurements of the base and height assuming a spherical drop. Measurements were performed at 23 °C and 50% RH with Milli-Q water. The contact angle was determined at three different positions on each sample. The values reported were taken after the contact angle had reached a stable value, typically less than 10 s after deposition of the droplet. Typical uncertainties in the experiments were ±4°.

X-ray photoelectron spectroscopy

The X-ray photoelectron spectroscopy (XPS) spectra were collected with a Kratos Axis Ultra DLD electron spectrometer (UK) using a monochromated A1 K_α source operated at 150 W, with a pass energy of 160 eV for wide spectra and a pass energy of 20 eV for individual photoelectron lines. The surface potential was stabilized by the spectrometer charge neutralization system. Photoelectrons were collected at a take-off angle of 90° relative to the sample surface which means a depth of analysis of ca. 10 nm. The binding energy (BE) scale was referenced to the C 1*s* line of aliphatic carbon, set at 285.0 eV. Three measurements were made on the silane-treated NFC aerogel (30 min with octyltrichlorosilane). The first measurement was on top of the aerogel, the second at the bottom and the third in the center of the aerogel after it had been sliced into two halves. The untreated aerogel was measured only once in the center.

Scanning electron microscopy

To study the micro-structure of the NFC aerogels, the specimens were studied with a Hitachi S-4800 field emission scanning electron microscope (FE-SEM) to obtain secondary electron images. The specimens were fixed on a metal stub with colloidal graphite paint and coated with a 6 nm thick gold/palladium layer using a Cressington 208HR High Resolution Sputter Coater.

Tomography

Microtomography was carried out using an Xradia MicroXCT-200. Scanning conditions: X-ray source: voltage 30 kV, power 6 W; number of projections 1,800, exposure time 3 s/projection. The distances from detector and X-ray source were 7 and 30 mm respectively, the magnification was 10× and the pixel resolution 2.18 μm. The analysed volume was 2 mm × 2 mm × sample thickness.

Nitrogen adsorption/desorption measurements

Specific surface areas were determined by N_2 adsorption/desorption measurements at the temperature of liquid nitrogen (ASAP 2020, Micromeritics, US). Before measurement, the samples were stored at a temperature of 117 °C until a vacuum of $<10^{-5}$ mmHg was reached. Both adsorption and desorption isotherms were measured and the surface area was determined from the adsorption results using the Brunauer-Emmet-Teller (BET) method. The error was less than 0.5 m^2/g.

Results and discussion

By altering the concentration of the NFC dispersion, aerogels with four different densities were prepared by vacuum freeze-drying. They were compared with regard to wetting properties, sorption ability and mechanical rigidity. The resulting densities ranged from 0.004 to 0.014 g/cm^3 and the porosities from 99.8 to 99.1%, see Table 1. The porosity has been calculated using the relationship $\phi = 100\left(1 - \frac{\rho_a}{\rho_s}\right)$ where ρ_a is the density of the aerogel and ρ_s is the

Table 1 Properties of aerogels made from NFC dispersions of different concentrations

wt% NFC	ρ (g/cm^3)	Porosity (vol%)	Specific surface area (m^2/g)
0.5	0.004	99.8	42
1	0.008	99.5	16
1.5	0.011	99.3	14
2	0.014	99.1	11

Specific surface area measured according to the BET method

density of crystalline cellulose (1.5 g/cm^3) (Eichhorn and Sampson 2010).

The aerogels were silanated with octyltrichlorosilane by vapor deposition in order to make them hydrophobic. Before treatment they could all be fully wetted with water, but the silane-coating reduced the surface energy and all four coated aerogels showed contact angles of approximately 150°. Non-polar liquids are however completely absorbed into the structure within 0.1 s after application, so that these aerogels can float on water and at the same time rapidly absorb non-polar liquids (as shown in Figs. 1, 2, 4, 5 and in movies included in the supporting information).

In order to evaluate the evenness of the result of the silane treatment through the aerogel, XPS analysis was used to determine the compositions on the top face, the inner phase and the bottom phase of the aerogel, in relation to the positioning of the aerogel during silane treatment. The atomic surface concentration of pure NFC aerogel and their modified analogues are displayed in Table 2. Carbon, oxygen and very small amounts of Na as counter ion to the carboxymethylated cellulose fibrils were detected on the surface of the unmodified cellulose, whereas the modified samples clearly showed the presence of silicon particularly on the top and the bottom surfaces of the aerogels.

Table 2 Atomic surface concentrations on non-treated and octyltrichlorosilane-treated NFC aerogels

	Surface concentration (%)			
	C	O	Na	Si
Untreated	61.3	38.2	0.6	
Top	86	9		5
Center	61	37	0.6	1
Bottom	88	7		5

Table 2 also shows that the center region of the treated aerogels was essentially unaffected by the

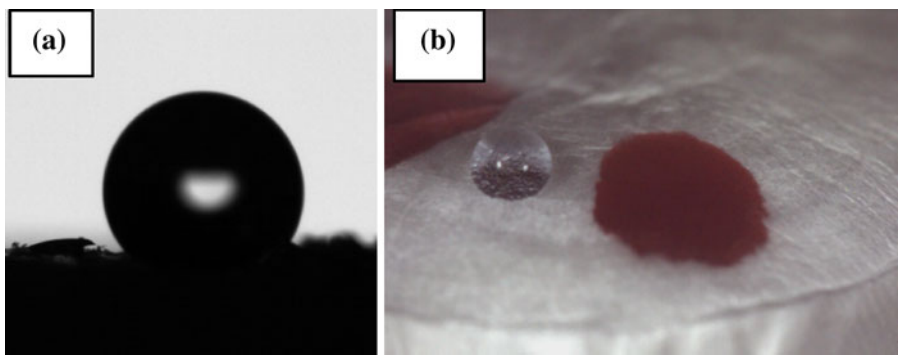

Fig. 1 **a** A water drop placed on top of an octyltrichlorosilane-treated aerogel consisting of 1 wt% NFC. The contact angle is 150° ± 4°. **b** A drop of hexadecane is totally and rapidly absorbed into the aerogel. A water droplet is resting on top of the material to the left of the hexadecane application point

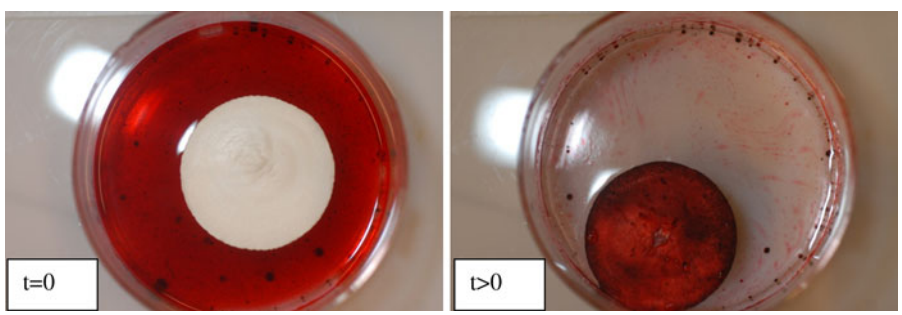

Fig. 2 A treated aerogel is able to float on water and simultaneously absorb a non-polar liquid (hexadecane, coloured red) distributed on top of the water phase. The aerogel used in these experiments had been prepared from a 1 wt% NFC dispersion and it could be removed after the absorption without losing its integrity

silane treatment, the 1% Si detected being probably due to unavoidable contamination during sample handling. The fact that the aerogels float on water even when all the oil has been absorbed indicates that the depth of the silane treatment is sufficient to render the aerogels permanently superhydrophobic. There is no established definition of this term, but it is usually required that the apparent contact angle is high and that the contact angle hysteresis is very low. As shown in Fig. 1, the apparent contact angle is 150°, which is high, but due to the highly porous structure of the aerogels it is very difficult to determine a receding contact angle with precision. However, the water droplets easily roll off the aerogels as soon as there is a slight increase in sliding angle, and it is thus considered safe to say that the aerogels are superhydrophobic. This was discussed earlier (Aulin et al. 2010b) where it was also shown that by treating the aerogels with fluorinated silanes it is possible to make the aerogels superoleophobic. Since a flat cellulose surface was found to have an advancing contact angle of 116° and since the images in 3a and b demonstrate the porous structure and rough surface of the aerogel, it is clear that it is the surface structure of the aerogel together with the hydrophobicity introduced by the silane treatment that is the explanation of the observed wetting behavior. This also agrees with earlier discussions about the superhydrophobic properties of modified cellulose aerogels (Aulin et al. 2010b; Kettunen et al. 2011).

During the experiments illustrated in Fig. 2 it was observed that the aerogels have a large liquid-holding capacity and that without any noticeable change in structure they could hold a volume of non-polar liquid many times their own weight. In order to characterize the liquid-holding properties of the aerogels, they were subjected to a pore size analysis using a liquid absorption/extrusion technique (Miller and Tyomkin 1994) where the relationship between pore size and liquid-holding capacity can be established. The results of these measurements are shown in Figs. 4 and 5 for aerogels with different solids contents. The pore radius shown on the x-axis is calculated from the chamber pressure and the Laplace equation assuming that the contact angle between hexadecane and cellulose is 0° and that the pores are cylindrical.

During these experiments a cumulative pore volume distribution is measured by liquid intrusion (sorption mode) and liquid extrusion (desorption mode), in these cases using hexadecane. After mounting the samples in the measuring chamber a cumulative pore volume distribution was recorded on the initially dry sample in sorption mode. After the initial wetting of the sample, subsequent sorption and desorption cycles were recorded on the wetted sample. The repeated measurement of several sorption/desorption cycles, starting with an initially dry sample, give information on both the liquid holding capacity of the small pores outside the measuring range of the equipment and on the sorption/desorption hysteresis. Also, any change in sample structure is tracked during the sorption/desorption measurement by the use of a height gauge registering changes in sample height.

As shown in Fig. 4, the average pore radius of the aerogels is 20–30 μm and there are considerable numbers of pores smaller than 20 μm and larger than 30 μm. This agrees with the scanning electron microscopy (SEM) image in Fig. 3b although it is

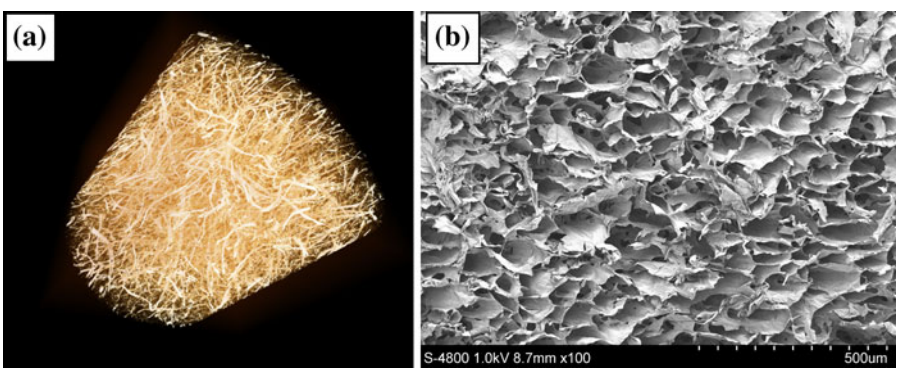

Fig. 3 **a** A 3-D Microtomography image of a 1 wt% NFC aerogel (see also supporting information for a 3-D animation). **b** FE-SEM image of a 1 wt% NFC aerogel where the scale bar is 500 μm

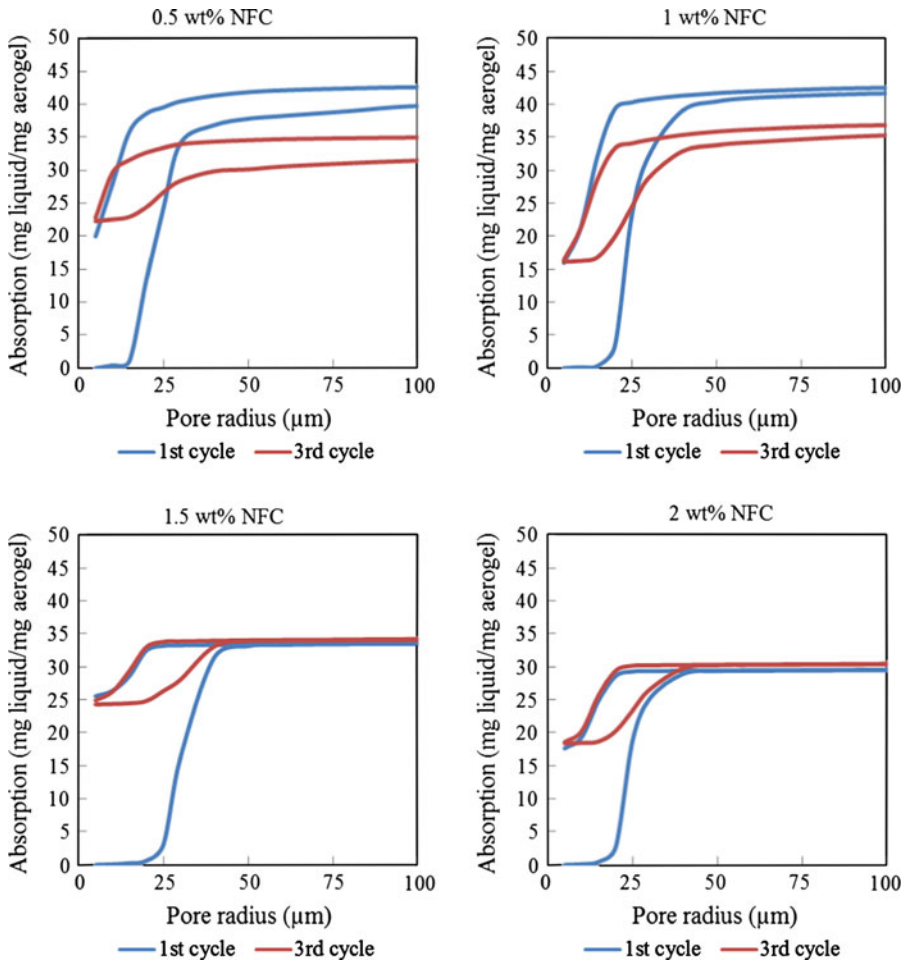

Fig. 4 Absorption and desorption of hexadecane into octyltrichlorosilane-treated aerogels prepared from gels with a solids content of 0.5–2 wt%. In these experiments, the dry aerogels were placed inside the test-chamber and hexadecane was allowed to enter into the aerogel as the pressure inside the chamber was decreased. The pore radius was calculated from the pressure inside the chamber and the Laplace equation, assuming that the contact angle between hexadecane and cellulose is 0°

very difficult to quantify the pore size and pore-size distribution from such images, 3b. A detailed inspection of the data also shows that the aerogels formed at a higher solids content have smaller average pore size and that there are no pores larger than 40 μm in the aerogels formed at 1 wt% and higher.

For all aerogels a hysteresis was observed between the sorption and desorption cycle. This was interpreted as being due to the presence of bottle-neck pores which become filled and emptied at different pressures due to their non-uniform distribution of radii along the paths traversed by the liquid during sorption and desorption. Furthermore, since the curves recorded for the first sorption cycle do not coincide with subsequent desorption and sorption cycles at the lowest pore sizes, i.e. the highest pressure, some of the liquid sorbed by the initially dry sample became permanently trapped in pores with effective radii smaller than the limiting pore radius of 5 μm. These interpretations are also consistent with the absence of non-coinciding sorption and desorption curves at the smallest pore size for higher sorption/desorption cycles. In this study gas pressure was used to empty the aerogels from oil but in the study made by Korhonen et al. (2011) they show that octane can effectively be used to release paraffin oil without losing the integrity of the aerogel.

The difference in recorded cumulative volume during sorption between the first and the third sorption cycle can both be due to the amount of non-polar liquid that is trapped in small pores and due to a collapse of the aerogel during sorption and desorption. In order to clarify this, the thickness of the aerogel was monitored during the measurements and the results are shown in Fig. 5, where the thickness has been

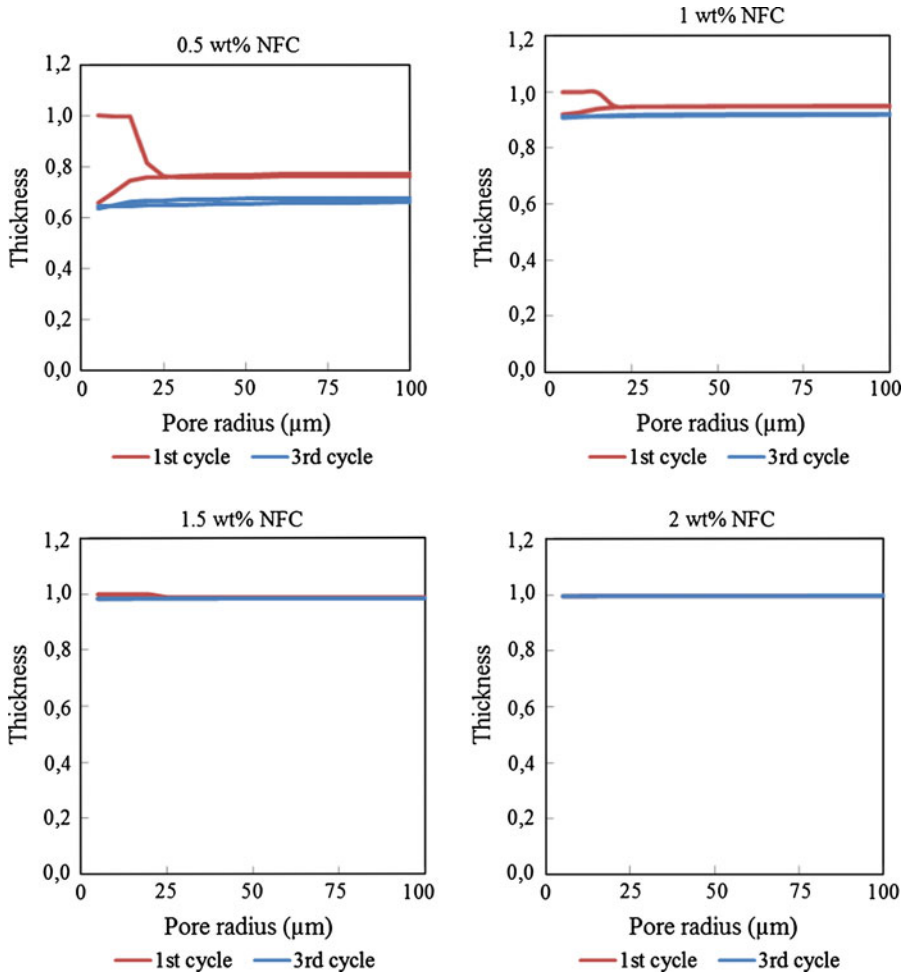

Fig. 5 Mechanical rigidity of the four different aerogels measured by changes in height upon liquid sorption and desorption. The thickness has been normalized with respect to the initial thickness of the aerogels

normalized with respect to the initial thickness of the aerogels. In the case of the aerogel formed at 0.5 wt% the absorption/desorption influences the thickness of the aerogel. As the hexadecane is sorbed, the thickness of the aerogel decreases (cycle 1 in Fig. 5, 0.5%) and during the desorption process there is a further decrease in the thickness, especially when the pressure in the chamber is increased to empty the smallest pores (cycle 3 in Fig. 5, 0.5%). A comparison of the thickness in the third absorption cycle with the thickness in the first desorption cycle shows that there is a permanent loss in thickness for this aerogel. In the case of the aerogels formed at higher solids contents, there is virtually no change in thickness during sorption and desorption. Table 3 shows that, despite the very high porosities of the aerogels formed at 1–2 wt%, they exhibit a structural integrity during sorption and desorption cycling with hexadecane. This

Table 3 Thickness changes during the first and third absorption cycles in the different aerogels

Solids content during aerogel formation (wt%)	Initial thickness (mm)	Relative thickness after first absorption	Relative thickness after third absorption
0.5	8.90	0.66	0.64
1.0	10.8	0.92	0.91
1.5	11.9	0.99	0.98
2.0	11.6	1.00	1.00

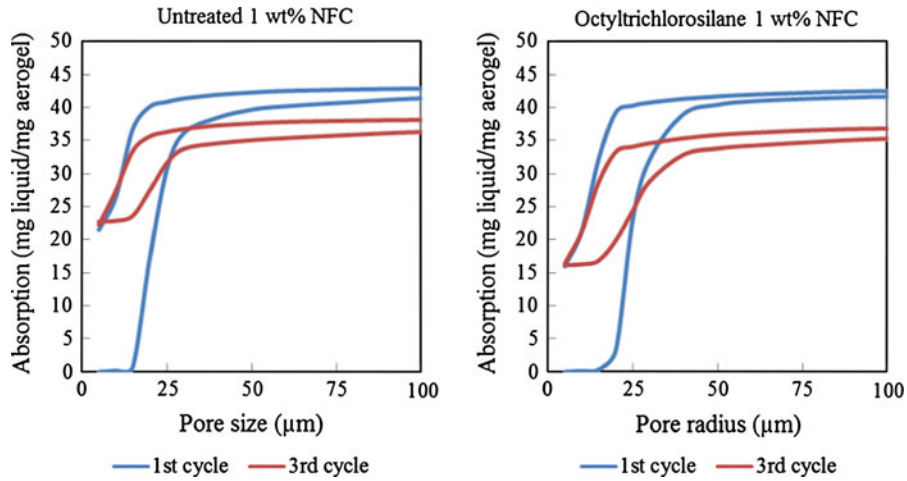

Fig. 6 Influence of the octyltrichlorosilane treatment on the sorption and desorption of hexadecane in aerogels formed at a solids content of 1 wt%

is related to their high mechanical strength (Sehaqui et al. 2010) and the fact that non-polar liquids do not affect the interaction between the cellulose fibrils to any great extent.

Since one of the main objectives of the present work was to investigate whether the aerogels could be functionalized to be superhydrophobic while maintaining their oil-absorbing capacity, it was important to clarify how the chemical treatment affected the absorption capacity with respect to non-polar liquids. Figure 6 shows that the octyltrichlorosilane treatment has only a minor negative influence on the absorption capacity of the aerogels.

Conclusions

A low density and highly porous material (>99%) for the effective separation of mixtures of non-polar and polar liquids has been prepared by chemical modification of NFC aerogels prepared by the freeze-drying of NFC dispersions. In order to render the porous materials hydrophobic, they were exposed to vapor-phase deposition of octyltrichlorosilanes which gave an aerogel with an advancing contact angle for water of 150°. Non-polar liquids could be imbibed into the aerogels and the absorption capacity of the material was up to 45 times its own weight. The aerogels can be reused several times and they show no significant change in volume upon sorption/desorption. The material is superhydrophobic and can therefore float on water and at the same time absorb non-polar liquids to function as a separation medium.

Acknowledgments The authors thank Wallenberg Wood Science Center for financial support. Professor Lars G. Ödberg is acknowledged for valuable discussions and Magnus Hillergren for professional help with the high speed camera. Joanna Hornatowska at Innvenita AB is acknowledged for the tomography measurements and Innventia AB is thanked for supplying NFC. Dr. Andrei Shchukarev at Umeå University is acknowledged for performing the XPS experiments.

References

Aulin C, Johansson E, Wagberg L, Lindstrom T (2010a) Self-organized films from cellulose I nanofibrils using the layer-by-layer technique. Biomacromolecules 11(4):872–882. doi:10.1021/bm100075e

Aulin C, Netrval J, Wagberg L, Lindstrom T (2010b) Aerogels from nanofibrillated cellulose with tunable oleophobicity. Soft Matter 6(14):3298–3305

Cervin NT, Aulin C, Wagberg L, Larsson T (2011) Hydrophobic aerogels from nanofibrillated cellulose (NFC) with tunable oleophilicity. Abstracts of Papers of the American Chemical Society, vol 241. p 81

Eichhorn SJ, Sampson WW (2010) Relationships between specific surface area and pore size in electrospun polymer fibre networks. J R Soc Interface 7(45):641–649. doi:10.1098/rsif.2009.0374

Henriksson M, Berglund LA, Isaksson P, Lindstrom T, Nishino T (2008) Cellulose nanopaper structures of high toughness. Biomacromolecules 9(6):1579–1585. doi:10.1021/bm800038n

Herrick FW, Casebier RL, Hamilton JK, Sandberg KR (1983) Microfibrillated cellulose: morphology and accessibility. J Appl Polym Sci 37:797–813

Hrubesh LW (1998) Aerogel applications. J Non-Cryst Solids 225(1–3):335–342. doi:10.1016/s0022-3093(98)00135-5

Kettunen M, Silvennoinen RJ, Houbenov N, Nykanen A, Ruokolainen J, Sainio J, Pore V, Kemell M, Ankerfors M, Lindstrom T, Ritala M, Ras RHA, Ikkala O (2011)

Photoswitchable superabsorbency based on nanocellulose aerogels. Adv Funct Mater 21(3):510–517. doi:10.1002/adfm.201001431

Korhonen JT, Kettunen M, Ras RHA, Ikkala O (2011) Hydrophobic nanocellulose aerogels as floating, sustainable, reusable, and recyclable oil absorbents. ACS Appl Mater Interfaces 3(6):1813–1816

Miller B, Tyomkin I (1994) Liquid porosimetry—new methodology and applications. J Colloid Interface Sci 162(1):163–170. doi:10.1006/jcis.1994.1021

Nakagaito AN, Yano H (2004) The effect of morphological changes from pulp fiber towards nano-scale fibrillated cellulose on the mechanical properties of high-strength plant fiber based composites. Appl Phys A-Mater Sci Process 78(4):547–552. doi:10.1007/s00339-003-2453-5

Paakko M, Ankerfors M, Kosonen H, Nykanen A, Ahola S, Osterberg M, Ruokolainen J, Laine J, Larsson PT, Ikkala O, Lindstrom T (2007) Enzymatic hydrolysis combined with mechanical shearing and high-pressure homogenization for nanoscale cellulose fibrils and strong gels. Biomacromolecules 8(6):1934–1941

Paakko M, Vapaavuori J, Silvennoinen R, Kosonen H, Ankerfors M, Lindstrom T, Berglund LA, Ikkala O (2008) Long and entangled native cellulose I nanofibers allow flexible aerogels and hierarchically porous templates for functionalities. Soft Matter 4(12):2492–2499. doi:10.1039/b810371b

Pekala RW (1989) Organic aerogels from the polycondensation of resorcinol with formaldehyde. J Mater Sci 24(9):3221–3227

Pekala RW, Farmer JC, Alviso CT, Tran TD, Mayer ST, Miller JM, Dunn B (1998) Carbon aerogels for electrochemical applications. J Non-Cryst Solids 225(1):74–80

Saito T, Nishiyama Y, Putaux JL, Vignon M, Isogai A (2006) Homogeneous suspensions of individualized microfibrils from TEMPO-catalyzed oxidation of native cellulose. Biomacromolecules 7(6):1687–1691. doi:10.1021/bm060154s

Sehaqui H, Salajkova M, Zhou Q, Berglund LA (2010) Mechanical performance tailoring of tough ultra-high porosity foams prepared from cellulose I nanofiber suspensions. Soft Matter 6(8):1824–1832. doi:10.1039/b927505c

Siqueira G, Bras J, Dufresne A (2009) Cellulose whiskers versus microfibrils: influence of the nature of the nanoparticle and its surface functionalization on the thermal and mechanical properties of nanocomposites. Biomacromolecules 10(2):425–432. doi:10.1021/bm801193d

Turbak AF, Snyder FW, Sandberg KR (1983) Microfibrillated cellulose, a new cellulose product: properties, uses and commercial potential. J Appl Polym Sci 37:815–827

Wagberg L, Decher G, Norgren M, Lindstrom T, Ankerfors M, Axnas K (2008) The build-up of polyelectrolyte multilayers of microfibrillated cellulose and cationic polyelectrolytes. Langmuir 24(3):784–795

Yano H, Sugiyama J, Nakagaito AN, Nogi M, Matsuura T, Hikita M, Handa K (2005) Optically transparent composites reinforced with networks of bacterial nanofibers. Adv Mater 17(2):153–155. doi:10.1002/adma.200400597